The Astrophysical Journal, 982:177 (10pp), 2025 April 1 https://doi.org/10.3847/1538-4357/adae89

Redshift Drift Effect through the Observation of the H I 21 cm Signal with SKA

Jiangang Kang[1,2], Tong-Jie Zhang[1,2], Peng He[3], and Ming Zhu[4]
[1] Institute for Frontiers in Astronomy and Astrophysics, Beijing Normal University, Beijing 102206, People's Republic of China; tjzhang@bnu.edu.cn
[2] School of Physics and Astronomy, Beijing Normal University, Beijing 100875, People's Republic of China
[3] Burerau of Frontier Science and Education, Chinese Academy of Sciences, Beijing 100190, People's Republic of China
[4] National Astronomical Observatories, Chinese Academy of Sciences, Beijing 100101, People's Republic of China
Received 2024 May 22; revised 2025 January 22; accepted 2025 January 24; published 2025 March 27

Abstract

This study presents the findings of using the Square Kilometre Array (SKA) telescope to measure redshift drift via the H I 21 cm signal, employing semiannual observational intervals within a redshift of around $z \sim 1$ with a main goal of directly gauging the Universe's expansion acceleration rate with mm s^{-1} precision. The SKA can detect over 1 billion H I 21 cm emissions from individual galaxies to redshift $z \sim 2$ and thousands of absorption lines from damped Lyα systems against bright quasars to redshift $z \sim 13$ with a sensitivity limit of 100 mJy. By utilizing SKA's high spectral resolution settings (0.001, 0.002, 0.005, 0.01 Hz) to detect redshift drift, particularly focusing on the 0.001 and 0.002 Hz configuration, one aims to achieve the necessary mm s^{-1} in precision measurement by the 0.5 yr observation period. The velocity drift rate, crucially determined by the two operational regimes within 0.01–0.21 mm s^{-1} and 0.031–0.17 mm s^{-1}, exceeds the theoretical accuracy limit of 1.28 mm s^{-1}. The analysis thoroughly restricts cosmological parameters related to dark energy using the Sandage–Loeb (SL) signal from the H I 21 cm emission and absorption lines. It estimates a H_0 of about 70 km s^{-1} Mpc^{-1}, Ω_m near 0.3, and w close to -1, w_0 around -1, and w_a approaching -0.1. These results strongly endorse the SL effect as an effective method for confirming cosmic acceleration and exploring the dark sector in real-time cosmology with the SKA.

Unified Astronomy Thesaurus concepts: Dark energy (351); Cosmology (343); Cosmological models (337); Accelerating universe (12); Extragalactic radio sources (508); Damped Lyα systems (349)

1. Introduction

The cosmological phenomenon of redshift drift, an observationally model-independent diagnostic also referred to as the Sandage–Loeb (SL) effect, signifies the temporal redshift fluctuations of extragalactic astrophysical sources. These fluctuations are predominantly scrutinized through detailed spectral analysis of the Lyα forest or the 21 cm hyperfine transition line absorption features in the spectra of intense radio-loud quasars (A. Sandage 1962; A. Loeb 1998; A. Balbi & C. Quercellini 2007; R. R. Caldwell & M. Kamionkowski 2009; A. G. Kim et al. 2015). The cosmological redshift drift serves as a pivotal diagnostic tool for examining the Universe's accelerated expansion, a phenomenon ascribed to the enigmatic dark energy. Characterizing the attributes of dark energy constitutes one of the paramount challenges in contemporary cosmology (A. G. Riess et al. 1998; S. Perlmutter et al. 1999; C. Quercellini et al. 2012).

Mapping the trajectory of cosmic evolution and elucidating the properties of dark energy (A. Balbi & C. Quercellini 2007; M. Martinelli et al. 2012; R.-Y. Guo & X. Zhang 2016; C. S. Alves et al. 2019; R. Cooke 2020; A. Heinesen 2021) or alternative cosmological constituents require the deployment of a multitude of observational methodologies. These include the photometric analysis of Type Ia supernovae (SNe Ia), the spatial characterization of acoustic oscillations in the cosmic microwave background radiation, and the identification of baryonic acoustic oscillations (BAOs) within the large-scale structure power spectrum, as well as observational phenomena such as weak gravitational lensing, gravitational-wave detections, and other probes. Significantly, the concept of cosmic redshift drift has been proposed as an innovative technique for the direct measurement of the Universe's acceleration, independent of any specific gravitational theories, spacetime curvature models, or clustering paradigms (S. Cristiani et al. 2023). Analyzing this cosmological phenomenon through its redshift dependence can elucidate certain enigmas inherent in fundamental theoretical frameworks (J. Kang 2021).

To achieve precise detection of the pure radial signal over a decadal timescale, it is essential to refine the experimental spectral precision to approximately cm s^{-1} or better. For annual velocity variations on the order of mm s^{-1}, the corresponding spectral frequency shift must be detected at or below the 0.1 Hz threshold. These stringent detection criteria are critical for an advanced single-dish radio telescope or an interferometric synthesis array. In the context of upcoming astronomical instrumentation, the European Southern Observatory's 40 m class Extremely Large Telescope (ELT) will conduct cosmological redshift drift measurements through the Lyα forest, specifically targeting redshift ranges $z = 2$ to $z = 5$. This will involve selecting high-redshift quasi-stellar objects as suitable candidates for these experiments. Over a two-decade observational period, the cumulative exposure will total 4000 hr, resulting in a radial velocity precision of 2.34 cm s^{-1}. This precision allows for the determination of the cosmological constant Ω_Λ to fall within the range [0.42, 0.74] with 95% confidence, assuming a spatially flat Universe and after marginalization over H_0 (J. Liske et al. 2008).

Promisingly, construction of the initial phase of the Square Kilometre Array (SKA1) commenced in 2021, strategically situated in the regions of South Africa and Australia. This phase accounts for roughly 10% of the projected full-scale

deployment of the subsequent Square Kilometre Array (SKA2). Upon its completion, the SKA is expected to be the foremost radio telescope, eclipsing all preceding instruments in capability, marking a significant technological leap a decade after the initiation of SKA1 (J. Lazio 2010; S. Rawlings & R. Schilizzi 2011; J. R. Pritchard & A. Loeb 2012; R. Braun et al. 2019; K. Spekkens et al. 2019; Square Kilometre Array Cosmology Science Working Group et al. 2020; M. Moresco et al. 2022). The SKA will facilitate real-time cosmological investigations by detecting the 21 cm emission from neutral hydrogen (H I) in galaxies within the redshift range of $0 < z < 1$. Particularly, the selection of face-on galaxies emitting a distinct single Gaussian spectral profile with a higher signal-to-noise ratio (S/N) will ensure the precision of the measured signal. In addition to investigating damped Lyα (DLA) systems through their absorption signatures observed against optimal radio backgrounds (N. Kanekar & F. H. Briggs 2004; S. Rawlings & R. Schilizzi 2011; H. R. Kloeckner et al. 2015; R. Morganti et al. 2015; L. Staveley-Smith & T. Oosterloo 2015; C. S. Alves et al. 2019; K. Bolejko et al. 2019; Y. Liu et al. 2020; M. Moresco et al. 2022; B. A. R. Rocha & C. J. A. P. Martins 2023), the experiment's advanced capabilities and increased sensitivity will substantially reduce the overall error of this signal. This will enable the survey to sample billions of H I galaxies at redshift $z < 2$ (H. R. Kloeckner et al. 2015; L. Staveley-Smith & T. Oosterloo 2015) and detect over 20,000 DLA systems at a redshift of approximately 2, given the 100 mJy flux threshold of the redshifted H I (neutral hydrogen) 21 cm absorption line (N. Kanekar & F. H. Briggs 2004). The Lyα forest at redshift $z < 1.65$ is intrinsically incapable of penetrating the Earth's atmosphere. However, at such redshifts, the Universe indicates the onset of or subsequent accelerated expansion, necessitating alternative observational methodologies to elucidate these anomalies. The presence of copious neutral hydrogen (H I) in the galactic peripheries results in the emission of 21 cm radiation, which remains unaffected by atmospheric interference. The dense, cold H I gas clouds within the intergalactic medium can absorb the redshifted 21 cm line emitted by background sources. Consequently, the SKA can leverage its superior spectral resolution and sensitivity to probe cosmic acceleration via H I 21 cm observations. This facilitates the investigation of dark energy evolution and the validation of cosmological models or constraints on parameter space.

The 21 cm line, alongside Lyα radiation emitted by neutral hydrogen atoms (H I) that are ubiquitous in both the interstellar medium and intergalactic medium, constitutes a prolific tool for the astronomical community. This emission line permits comprehensive analyses of the neutral hydrogen gas properties within galaxies, including their spatial distribution, mass, thermodynamic state, and kinematic characteristics. Moreover, this spectral feature allows astronomers to trace the evolutionary stages of galaxies and investigate cosmological phenomena through redshift measurements. The forthcoming H I survey by the SKA is projected to significantly enhance the cosmological volume probed by the 21 cm emission, enabling the resolution of 1 billion galaxies at a redshift of approximately $z \sim 2$, thereby extending our comprehension of the Universe. Operating in a low spectral resolution mode, the SKA is anticipated to catalog approximately 10^7 galaxies within a redshift range of 0.2–1. The observation of the H I 21 cm emission from extragalactic sources at considerable redshifts ($z > 0.1$) presents significant challenges due to the inherently weak signal and the current sensitivity limitations of radio telescopes (J. R. Allison et al. 2022). Nevertheless, DLA systems, characterized by neutral hydrogen column densities exceeding $2 \times 10^{20}\,\mathrm{cm}^{-2}$, have traditionally been regarded as the principal progenitors of spiral galaxies and the primary reservoirs of cosmic neutral gas mass at high redshift ($z \sim 3$). This correlation is partially substantiated by the presence of low-ionization Mg II absorption lines, which become observable in the ground-based optical range upon redshifting. It should be noted, however, that the galaxies associated with DLAs are not exclusively spiral galaxies; they also encompass dwarf galaxies and low surface brightness galaxies at lower redshifts (A. M. Wolfe 1988; W. Lane et al. 1998; N. Kanekar & J. N. Chengalur 2001; N. Kanekar et al. 2001; K. Geréb et al. 2015; R. Morganti et al. 2015). When radio galaxies or luminous quasars interact with dense H I gas clouds, significant self-shielding occurs at a critical column density, leading to the manifestation of a distinctive absorption feature at 1420.4 MHz within the clouds' continuum spectrum. These clouds typically reside in two categorically stable environments: the cold neutral medium, with temperatures spanning from 80 to 1000 K, and the warm neutral medium, with temperatures ranging from 5000 to 8000 K. The resultant spin temperature is derived as a weighted harmonic mean of the temperatures of the various phases within a multiphase medium, dictated by the observed column density (N. Kanekar et al. 2001; N. Gupta et al. 2013; J. R. Allison et al. 2022). Employing the H I 21 cm absorption spectra as a diagnostic tool for probing cosmic expansion offers a promising trajectory for contemporary cosmology owing to its resilience against atmospheric disturbance and insensitivity to redshift effects, thereby facilitating ground-based telescopic observations (N. Kanekar & F. H. Briggs 2004; J. Liske et al. 2008; J. Darling 2012; H.-R. Yu et al. 2014; P. Mishra & T. P. Célérier Marie-Noëlle Singh 2015; K. Bolejko et al. 2019; R. Cooke 2020; K. Jiao et al. 2020; C. J. A. P. Martins et al. 2021; C.-Z. Lu et al. 2022; S. Cotsakis et al. 2023; J. Kang et al. 2023; B. A. R. Rocha & C. J. A. P. Martins 2023).

The primary aim of this investigation is to estimate the accuracy of determining the redshift drift rate as a metric for measuring cosmic expansion. This is accomplished through the utilization of the SKA to observe the H I 21 cm spectral emission and absorption over an observational time frame of $\Delta t = 0.5$ yr. The study subsequently strives to enhance the precision of cosmological parameters within the ΛCDM, wCDM, and Chevallier-Polarski-Linder (CPL) frameworks at an approximate redshift of $z \sim 1$. The manuscript is structured as follows. Section 1 delivers an extensive overview of the redshift drift phenomenon, the characteristics of the H I 21 cm spectral line, and the observational methodologies employed by the SKA. Section 2 expounds on the theoretical basis of the SL test and cosmic acceleration models and summarizes the systematic effects and target selection criteria in Section 3. Section 4 presents the empirical results derived from the constraints imposed by H I 21 cm data on cosmological parameters. Finally, Section 5 encapsulates the significant conclusions of the research.

2. Redshift Drift Effect Model

The cosmological redshift drift represents a crucial metric for assessing the spacetime expansion within the context of observational cosmology. This phenomenon can be

theoretically described as follows:

$$\dot{z}_s = \frac{\Delta z}{\Delta t} = H_0(1+z) - H(z). \quad (1)$$

Within the specified cosmological paradigm, the Hubble parameter, $H(z)$, denotes the Universe's expansion rate at a given redshift, z. This rate is quantitatively defined as the ratio of the derivative of the scale factor with respect to time, $\dot{a}$, to the scale factor, a. $H(z)$ encapsulates the dynamics inherent to the selected cosmological model, while H_0 represents the Hubble constant, indicative of the present expansion rate. The observable signal is frequently articulated in terms of the spectroscopic radial velocity shift, Δv, mathematically described by $\Delta v = c\Delta z_s/(1+z_s)$, where c denotes the speed of light and Δz_s signifies the variation in spectroscopic redshift z_s:

$$\dot{v} = \frac{\Delta v}{\Delta t} = c\frac{H_0}{1+z_s}\left[1 + z_s - \frac{H(z_s)}{H_0}\right]. \quad (2)$$

Similarly, the frequency shift over an observation interval Δt for a comoving source, as derived from $\nu_1 = \nu_{21}/(1+z)$ and $\nu_2 = \nu_{21}/(1+z+\Delta z)$, can be expressed as

$$\Delta\nu = \nu_2 - \nu_1 \approx -\nu_{21}\frac{\Delta z}{(1+z)^2}. \quad (3)$$

In this context, $\nu_{21} = 1420.405751768$ MHz represents the rest-frame frequency of the H I 21 cm absorption line, with z indicating the initially determined redshift and ν_2 and ν_1 denoting the first and second observed frequencies, respectively.

It is well known that the Universe is experiencing a phase of acceleration at a redshift close to $z = 0.67$, having transitioned from a previous era of deceleration. Consequently, the velocity drift exhibits positive values at lower redshifts, inversely shifting to negative values as redshift increases (C. J. A. P. Martins et al. 2021; J. Kang et al. 2023). The limiting velocity drift resulting from a time interval of $\Delta t = 0.5$ yr with the full SKA configuration is approximately 1.28 mm s^{-1} within the redshift range $z \sim 1$. It is anticipated that the experiment will be conducted using high spectral resolution data sets ($\Delta\nu = 0.001$, 0.002, 0.005, 0.01 Hz) to further investigate this phenomenon (H. R. Kloeckner et al. 2015; C. S. Alves et al. 2019; Y. Liu et al. 2020). It is crucial to acknowledge that, regarding the feasibility of utilizing the H I 21 cm signal, only spectral resolutions of $\Delta\nu = 0.001$ and 0.002 Hz can achieve the necessary accuracy throughout the entire redshift range of $z = 0$–1. Figure 1 delineates the necessary precision for redshift measurements and the detection of frequency shifts over observational intervals of 0.5 and 1 yr, respectively, as forecasted by the standard ΛCDM cosmological model based on the Planck 2018 data release (P18; Planck Collaboration et al. 2020). The graph indicates that the redshift measurement precision Δz reaches an average magnitude of approximately 10^{-11} on the left ordinate, while the frequency resolution $\Delta\nu$ on the right ordinate achieves a subhertz level, specifically below 0.1 Hz, over observational periods of either half a year or a full year. This enhanced resolution, enabled by the SKA and reduced observation intervals, imposes the spectral discrimination and requisite stability for the detection of the SL signal.

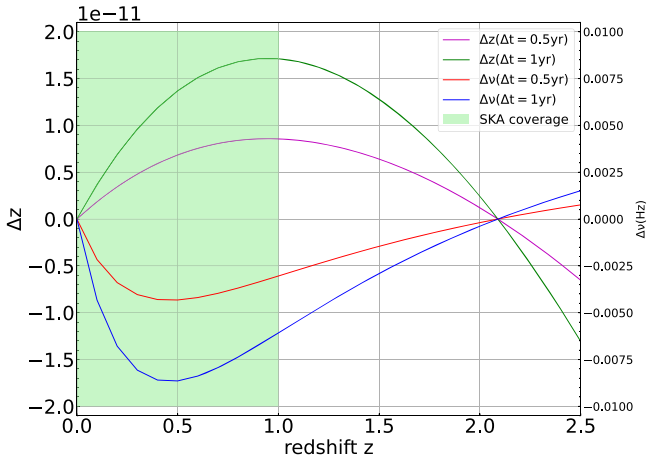

Figure 1. Theoretical variations of redshift drift Δz (left) and frequency resolution $\Delta\nu$ (right) as functions of redshift, considering an observational duration of 0.5 and 1 yr within the framework of ΛCDM cosmology (P18). The light green region delineates the redshift range accessible to SKA observations.

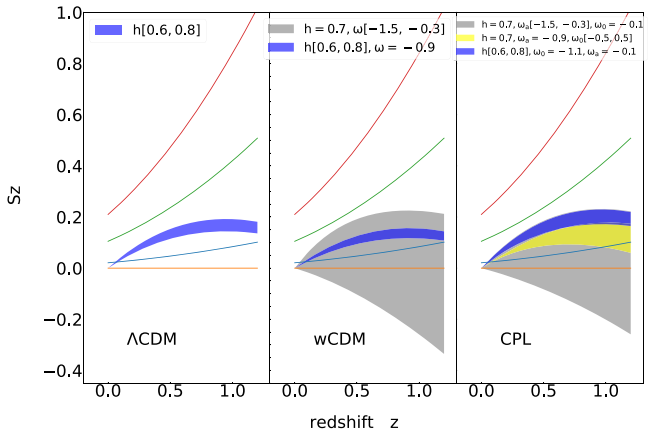

Figure 2. The variation of the dimensionless redshift drift with different cosmological models and redshifts is depicted, where the colored lines from bottom to top denote the spectral resolution capabilities of the SKA (0.001, 0.002, 0.005, 0.01 Hz), and the shaded regions in various colors indicate the ranges of specific parameter variations.

Considering the spectral resolution capabilities of the SKA at 0.001, 0.002, 0.005, and 0.01 Hz, we rigorously define the quantification of the dimensionless redshift drift, denoted as S_z, and the velocity drift, indicated as S_v, following the definitions established in prior research (C. S. Alves et al. 2019; C. J. A. P. Martins et al. 2021):

$$Sz = \frac{1}{H_{100}}\frac{\Delta z}{\Delta t} = h[1 + z - E(z)], \quad (4)$$

$$Sv = \Delta v = kh\left[1 + \frac{E(z)}{1+z}\right]. \quad (5)$$

In this context, $H_0 = hH_{100}$, where H_{100} represents 100 km s^{-1} Mpc^{-1}, and $E(z) = H(z)/H_0$. The parameter $k = cH_{100}\Delta t$. Figures 2 and 3 illustrate the two variables within the ΛCDM, wCDM, and CPL cosmological models. The two graphical depictions demonstrate that, within the intrinsic uncertainties of the Hubble constant H_0 ranging from 60 to 80 km s^{-1} Mpc^{-1}, spectral resolutions of 0.001 and 0.002 Hz are plausible scenarios for the unequivocal detection

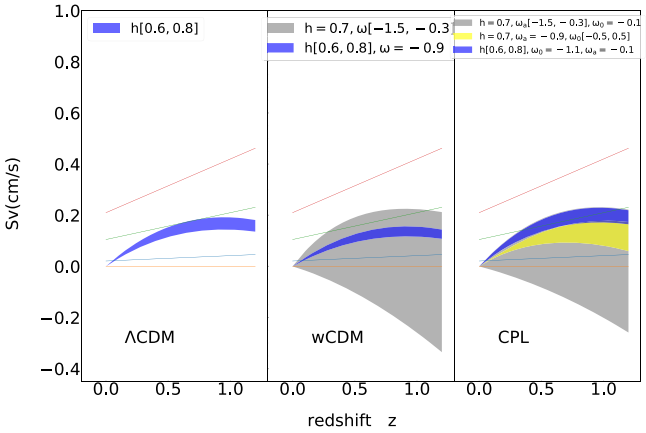

Figure 3. The variation in dimensionless velocity drift as a function of specific models and redshift is illustrated by four distinct lines from bottom to top, corresponding to the spectral resolution capabilities of the SKA (0.001, 0.002, 0.005, 0.01 Hz). The shaded regions in different colors represent the range of specific parameter variations.

Table 1
Values of Dimensionless Redshift Drift and Velocity Drift

Quantity	Mode	ΛCDM	wCDM	CPL
Sz	th	[0, 0.3]	[−0.4, 0.4]	[−0.35, 0.35]
	obs		[0, 0.65]	
Sv	th	[0.0, 0.15]	[−0.2, 0.2]	[−0.14, 0.18]
	obs		[0.02, 0.48]	

Note. The magnitude of the dimensionless redshift drift and velocity drift derived from theoretical predictions and observational data, as depicted in Figures 2 and 3, under three distinct cosmological models are represented by "th" and "obs," respectively.

of signals spanning the entire redshift range from 0 to 1. This achieves observational precision levels of 0.21–0.42 mm s^{-1} and 0.42–0.84 mm s^{-1}, respectively, and accommodates fluctuations in the dark energy equation-of-state parameters w, w_0, and w_a. The corresponding color-coded maps in blue, gray, and yellow illustrate these specific parameter variations as indicated in the legend, while the numerical values associated with these specific parameter variations are detailed in Table 1.

3. Systematic Effects and Target Selection

Systematic effects encompass the stability of baseline and frequency calibration; the relative angular displacement of absorbing gas with respect to background objects; variations in the illumination source's size, flux, and spectral characteristics; observer motion, peculiar velocities, and accelerations; and gravitational accelerations within and between targeted objects. The necessary calibration stability is contingent on a local oscillator, and current radio facilities are capable of supporting this level of precision (R. Cooke 2020). If experiments are conducted in a highly noninertial reference frame with multiple accelerations and rotations, the precision will be thoroughly addressed in the SKA era, potentially surpassing the requirements for signal detection (A. G. Kim et al. 2015; H. R. Kloeckner et al. 2015; C. S. Alves et al. 2019; R. Cooke 2020; M. Moresco et al. 2022). Moreover, the sign of $\dot{z}$, a well-documented phenomenon at both low and high redshifts (deviating from the null value), and the directions of gravitational accelerations are stochastic and null-centered. Consequently, the cumulative impact of peculiar accelerations will be mitigated by expanding the H I 21 cm sample sizes across diverse sky regions, increasing integration time, and extending the duration of the experiments (M. Moresco et al. 2022). Regarding the feasibility of experiments with the SKA (H. R. Kloeckner et al. 2015), for extragalactic sources with redshifts exceeding 0.2, the peculiar motion in redshift space will be attenuated to 10^{-14}, which is an order of magnitude lower than the percent-level cosmological signal and can be disregarded in forthcoming observations.

In addition to the frequency stability and gravitational accelerations of H I 21 cm signals, numerous technical constraints need thorough examination, broadly classified into three categories. First, the observation will be conducted within an ultrastable reference framework, with no temporal or positional deviations relative to the targets. Astrometric accuracy, time standards, and pointing precision must be calibrated and adjusted to an accuracy of 1″. These inevitable interferences will be systematically addressed as data streams from spectral channels into processing pipelines. Second, pulsar observations provide an unbiased solution due to their precise timing capabilities, allowing for long-term stability assessments of the global SKA system by analyzing the pulse arrival times of multiple pulsars to eliminate systematic effects. Additionally, a vast number of correlator channels will be employed to comprehensively capture the neutral hydrogen signals of spiral galaxies. Determining the redshift drift requires 10^8–10^9 correlator channels, a challenge that can be effectively managed through meticulous spectral window design and frequency standardization during data acquisition (H. R. Kloeckner et al. 2015; Square Kilometre Array Cosmology Science Working Group et al. 2020).

Assuming the precise identification of targeted samples can generate sufficient radiation at any redshift to achieve reasonable error margins of $\sigma_v \leqslant 1$ mm s^{-1} yr^{-1}, especially for emission line galaxies. For H I 21 cm emission, galaxies exhibiting a single Gaussian profile will be ideal targets, provided they have peak signals exceeding 100 mJy and an S/N of at least 100, due to the more stable baseline and superior sensitivity of the SKA system. Conversely, DLA systems with multiple Gaussian components will yield lower errors for SL signals, making intervening DLA systems the primary targets (A. M. Wolfe 1988; N. Kanekar & J. N. Chengalur 2001; N. Kanekar & F. H. Briggs 2004; J. Darling 2012; F. B. Abdalla et al. 2015; A. G. Kim et al. 2015; R. Morganti et al. 2015; L. Staveley-Smith & T. Oosterloo 2015; S. Yahya et al. 2015; R. Cooke 2020; Y. Liu et al. 2020; Square Kilometre Array Cosmology Science Working Group et al. 2020; J. R. Allison et al. 2022; R. Dutta et al. 2022; S. Cristiani et al. 2023; B. A. R. Rocha & C. J. A. P. Martins 2023; S. L. Eden et al. 2025; J. Kang et al. 2024; H. Yoon et al. 2024).

4. Result and Discussion

This section elucidates the methodologies employed for estimating velocity drift and its consequential implications for cosmology. In alignment with the findings depicted in Figure 4, the precision of velocity shift estimation can be achieved by leveraging the SKA's spectral capabilities of 0.001 and 0.002 Hz. Two configurations are thoroughly examined in detecting the 21 cm line emissions of neutral hydrogen (H I)

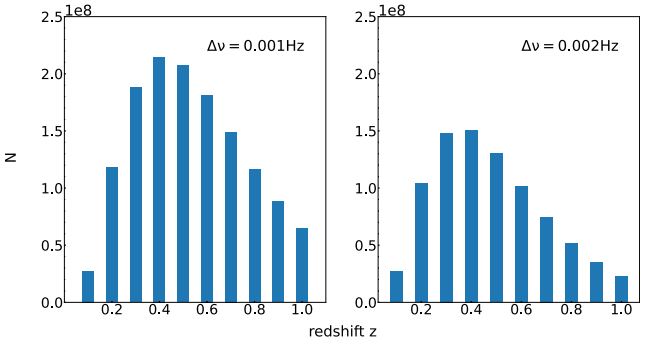

Figure 4. The redshift distribution of the number of extragalactic H I 21 cm emissions detected by SKA at a spectral resolution of 0.001 Hz (left) and 0.002 Hz (right).

from galactic sources, as well as the absorption features of DLA systems, over a redshift range of $0 < z < 1$. Regarding different cosmic epochs, specifically the epoch of cosmic evolution with redshift $2 < z < 5$, the ELT serves as a complementary instrument. Furthermore, constraints on H_0, Ω_m, and the dark energy equation-of-state parameters ω, ω_0, and ω_a are considered, taking into account the H_0 uncertainty spanning from 60 to 80 $\mathrm{km\,s^{-1}\,Mpc^{-1}}$. The chi-squared ($\chi^2$) distribution is applied to the velocity shift (Δv), which informs the posterior distribution used to compute the likelihood functions for the parameter sets within each respective model:

$$\chi^2 = \sum_{i=1}^{N} \frac{(\Delta v_{\rm obs} - \Delta v_{\rm th})^2}{\sigma_i^2}. \quad (6)$$

In the equation, $\Delta v_{\rm th}$ represents the theoretical velocity as delineated by Equation (2), whereas $\Delta v_{\rm obs}$ denotes the observed velocity for the ith data point, ascertained through SKA observations with ultrahigh spectral resolutions of 0.001 and 0.002 Hz, as referenced in H. R. Kloeckner et al. (2015). Additionally, $\sigma_{\rm i}$ signifies the standard error attributed to the ith data point, calculated as the reciprocal of the square root of the source count ($\sigma_{\rm i} \sim 1/\sqrt{N}$), where N denotes the number of galaxies or DLA systems detectable at these specified resolutions established on the SKA platform:

$$\frac{dN/dz}{\rm deg^2} = 10^{c_1} z^{c_2} \exp(-c_3 z), \quad (7)$$

$$b_{\rm HI}(z) = c_4 \exp(c_5 z). \quad (8)$$

The objective is to ascertain the velocity drift error, denoted as σ_i, through the utilization of the galaxies' redshift distribution. This can be accomplished by computing the detection distribution, represented by the function dN/dz, using the specific Equation (7), while the H I galaxy bias can be validated via Equation (8). The SKA conducts this analysis for each 0.1 redshift bin within the range of $z = 0$–1 (D. Obreschkow et al. 2009; S. Yahya et al. 2015). The coefficients c_1, c_2, c_3, c_4, and c_5 are variables associated with the respective detection limits, as indicated in Table 4 of S. Yahya et al. (2015). In our study, we utilize the constants c_1, c_2, c_3, c_4, and c_5 with values of (6.532, 1.932, 5.224, 0.530, 0.781) for the 0.001 Hz scenario and (6.555, 1.932, 6.378, 0.549, 0.812) for the 0.002 Hz case to determine the number of distant galaxies (N) detectable via the H I 21 cm emission line.

In Figure 4, the left panel demonstrates the SKA's proficiency in identifying extragalactic distributions with an exceptional spectral resolution of 0.001 Hz. For each 0.1 increment in redshift, there is an average density of 1.36×10^8 galaxies, with a peak density of approximately 2.14×10^8 galaxies at a redshift of 0.4 and a minimum of 2.8×10^7 galaxies at a redshift of 0.1. Cumulatively, at a spectral resolution of 0.001 Hz, the total number of galaxies observed up to a redshift of 1 is nearly 1.36 billion. In comparison, at a spectral resolution of 0.002 Hz, the maximum galaxy density is around 1.51×10^8 at a redshift of 0.4, with a cumulative count of approximately 8.46×10^8 galaxies by a redshift of 1 and a minimum of 2.69×10^7 galaxies within the redshift bin of 0.1. Upon analyzing galaxy counts, as the redshift z exceeds 0.4, a significant reduction is observed in both scenarios, highlighting the critical importance of distribution analysis in understanding galactic evolution and its cosmological implications. A comparative assessment reveals that the scenario with a spectral resolution of 0.001 Hz significantly outperforms the 0.002 Hz resolution across all redshift bins. The maximum discrepancy between these cases is observed at a redshift of approximately 0.6, where the count difference reaches 9.87 million, and by a redshift of around 1, the total divergence amounts to 5.09×10^8. Preferentially, face-on galaxies are utilized to determine the redshift drift effect due to their prominent single Gaussian emission profiles.

Consequently, the observed velocity drifts $\Delta v_{\rm obs}$ on the SKA can be quantified under the two spectral resolution scenarios of 0.001 Hz and 0.002 Hz. This quantification depends on the assessment of the total number of sources of H I 21 cm signals, N, within each redshift bin, z, encompassing both emission and absorption line data, as well as the observational duration, ΔT. This relationship can be precisely modeled as the following formalism (J. Liske et al. 2008; H. R. Kloeckner et al. 2015; C. S. Alves et al. 2019; K. Bolejko et al. 2019; J. Esteves et al. 2021; C. Dong et al. 2022):

$$\Delta v_{\rm obs} = \sigma_n N^{-1/2} (1 + {\rm z})^{\lambda} \Delta \nu^{1/2} \quad [{\rm cm\,s^{-1}}]. \quad (9)$$

The parameter σ_n denotes a normalization constant. For emissions from extragalactic sources, we project an approximate count of $N = 10^7$ per 0.1 redshift interval up to $z = 1$ over an observational duration of $\Delta T = 0.5$ yr, employing spectral resolutions of 0.001 Hz and 0.002 Hz within the redshift span $0 \leqslant z \leqslant 1$. The parameter λ is held constant at 1.09 for the 0.001 Hz data and 1.52 for the 0.002 Hz data set. In terms of detection accuracy, theoretical analyses indicate that with an observation period of $\Delta T = 0.5$ yr, the SKA is capable of detecting redshift drift at spectral resolutions between 0.001 and 0.01 Hz (H. R. Kloeckner et al. 2015). It is optimal for the data precision not to exceed 0.002 Hz as the redshift approaches unity. The normalization constant σ_n ranges from 1 to 5 $\mathrm{cm\,s^{-1}}$, varying with spectral resolution and redshift (J. G. Kang et al. 2024, in preparation), and decreases linearly in both contexts. At lower redshifts or spectral resolutions, the values are notably higher, especially when the redshift exceeds 0.8 or the spectral resolution surpasses 0.01 Hz, maintaining a constant error margin of 0.25. Consequently, the substantial number of targeted sources with adequate S/Ns (S/N > = 100) during the SKA era will guarantee the experiment's reliability.

Figure 5 illustrates the velocity drift values, denoted as $\dot{\rm v}$, represented by green cross error bars, along with those derived from three distinct theoretical models that hypothesize a systematic deviation in the Hubble constant (H_0) ranging from

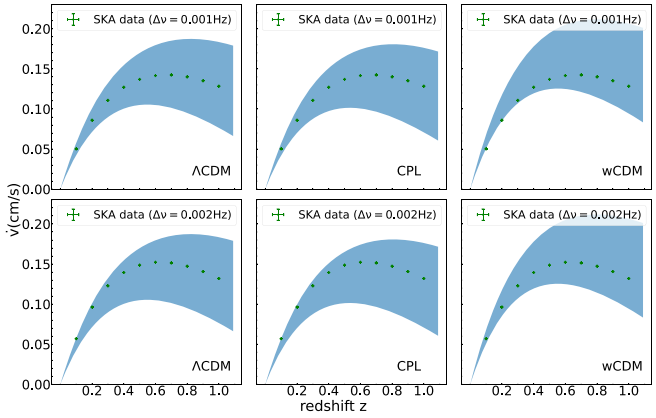

Figure 5. The light blue region in each graph represents the extent of velocity drift, taking into account the uncertainty in H_0 ranging from 60 to 80 km s^{-1} Mpc^{-1} over a 0.5 yr observation period within the redshift interval of 0–1. The observed redshift and velocity drift data from SKA, with spectral resolutions of 0.001 Hz (top panels) and 0.002 Hz (bottom panels) derived from the H I 21 cm emission of individual galaxies, are depicted with green cross error bars.

Table 2
The Priors Applied to the Free Parameters in the ΛCDM, wCDM, and CPL Cosmological Models

Parameter	Prior
H_0	[60, 80]
Ω_m	[0.1, 0.6]
w	[−3, 3]
w_0	[−3, 3]
w_a	[−3, 3]

60 to 80 km s^{-1} Mpc^{-1}, depicted in a shallow blue contour map. The top panels correspond to a frequency of 0.001 Hz, while the bottom panels pertain to a frequency of 0.002 Hz. The x-axis and y-axis denote the redshift drift and the velocity drift, respectively. Through semiannual observational analysis ($\Delta t = 0.5$ yr) as shown in the figure, the empirically determined velocity drift rates range from 0.05 to 0.15 cm s^{-1}, with the associated uncertainties quantified between 0.01 and 0.03 cm s^{-1}.

Regarding the recorded metrics of the two panels, the mean value derived from the 0.002 Hz frequency is marginally higher, by 0.003–0.007 cm s^{-1}, compared to the 0.001 Hz data, particularly at lower cosmological volumes. This degree of precision aligns perfectly with the predictions from various theoretical frameworks as outlined in Equation (2). As illustrated in Figure 6, within the ΛCDM and wCDM cosmological models, the analysis suggests a preference for a Hubble constant (H_0) around 70 km s^{-1} Mpc^{-1}. In contrast, under the CPL parameterization, the data indicate a slightly lower H_0 value, approximately 67 km s^{-1} Mpc^{-1}.

In relation to the emission findings, we impose constraints on the cosmological parameters within the frameworks of the standard ΛCDM, wCDM, and CPL parameterization models by leveraging the anticipated data from the 21 cm emission line. The prior distributions for these parameters are detailed in Table 2. The best-fit parameter estimates for H_0, Ω_m, w, w_0, and w_a are depicted along with their corresponding 68.3% (1σ) and

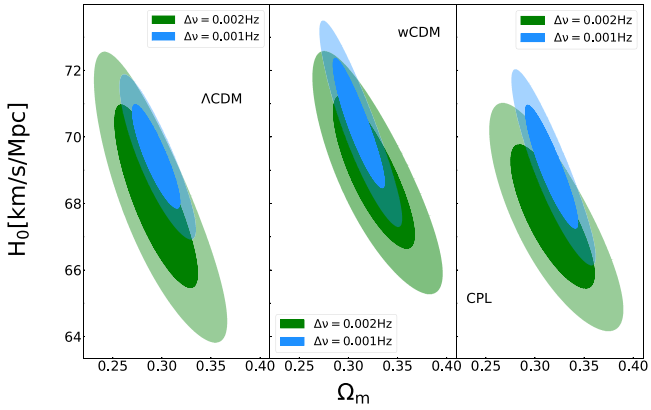

Figure 6. The constraints on the H_0 and Ω_m parameter space within the 1σ and 2σ confidence intervals, derived from the predicted data utilizing the SKA's spectral resolutions of 0.001 Hz (blue contours) and 0.002 Hz (green contours).

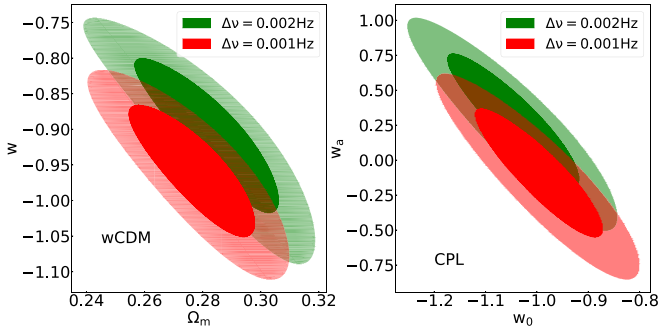

Figure 7. The constraints on w, w_0, and w_a within the 1σ and 2σ confidence intervals, derived from the forecasted data using the SKA spectral resolutions of 0.001 Hz (depicted by red contours) and 0.002 Hz (depicted by green contours).

95.4% (2σ) confidence levels in Figures 6 and 7 and Tables 3 and 4 for the 0.001 Hz and 0.002 Hz data, respectively. Analysis of the panels reveals that the constrained data are in close concurrence with results from other observational probes, with a significantly narrowed parameter space for all parameters, especially for H_0 and Ω_m in the CPL model.

Regarding the findings at 0.001 Hz and 0.002 Hz frequencies, the Hubble constant H_0 was confined within the range of 70.4–67.13 km s^{-1} Mpc^{-1}. The precision in the ΛCDM model has been enhanced, tightening from 1.12% to 0.8%. For the wCDM model, the precision has increased from 1.19% to 1.06%, and in the CPL model, from 0.91% to 0.84%. Furthermore, constraining the matter density parameter Ω_m within 0.294–0.328 yielded precision improvements as follows: in the ΛCDM model, from 1.05% to 0.88%; in the wCDM model, from 1.33% to 1.08%; and in the CPL model, from 1.52% to 1.17%. In the wCDM model, the accuracy of the dark energy equation-of-state parameter w has improved from 2.24% to 1.65%. In the CPL model, the precision of parameter w_0 has increased from 4.55% to 3.66%, and for w_a, the enhancement is from 4.30% to 3.61%. This indicates that parameter degeneracies are effectively mitigated when integrating SKA observations with other cosmological data sets.

With respect to the analysis predicated on H I 21 cm absorption, Figure 8 delineates the enumeration of DLA systems at an approximate redshift of $z \sim 1$, as identified by the SKA with a detection threshold sensitivity of 100 mJy via the H I 21 cm absorption line. The spatial density of DLA

Table 3
The Optimal Parameter Values and 1σ (68.3%) Confidence Intervals for Constraints at 0.001 Hz under Three Different Cosmological Frameworks

Model	H_0	Ω_m	w	w_0	w_a
ΛCDM	$69.6^{+1.07}_{-0.94}$	$0.311^{+0.304}_{-2.214}$	…	…	…
wCDM	$70.4^{+0.81}_{-0.72}$	$0.317^{+0.087}_{-0.142}$	$-0.953^{+0.077}_{-0.101}$	…	…
CPL	$69.3^{+1.22}_{-1.09}$	$0.324^{+0.284}_{-0.165}$	…	$-0.992^{+0.118}_{-0.251}$	$-0.124^{+0.385}_{-0.439}$

Table 4
The Optimal Value and 1σ (68.3%) Confidence Intervals for the 0.002 Hz Observational Data from SKA within the Framework of the Three Cosmological Models

Model	H_0	Ω_m	w	w_0	w_a
ΛCDM	$68.26^{+2.881}_{-3.046}$	$0.294^{+0.047}_{-0.028}$	…	…	…
wCDM	$69.24^{+2.902}_{-2.397}$	$0.321^{+0.087}_{-0.142}$	$-0.861^{+0.071}_{-0.153}$	…	…
CPL	$67.13^{+1.822}_{-1.453}$	$0.328^{+0.271}_{-0.193}$	…	$-1.03^{+0.130}_{-0.231}$	$0.244^{+0.264}_{-0.517}$

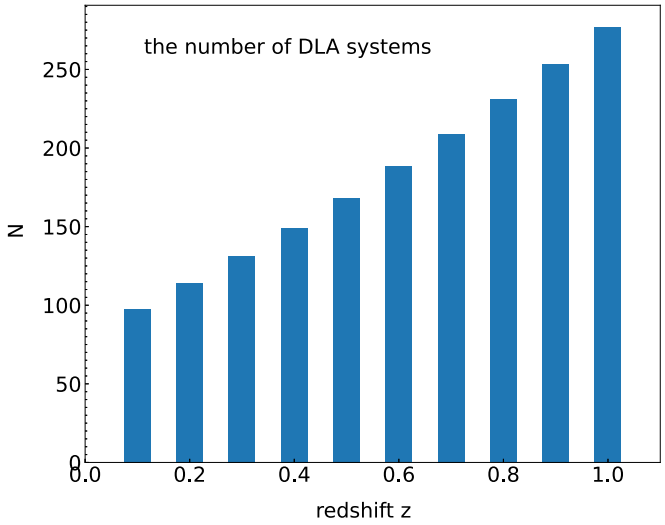

Figure 8. The census of DLA systems at redshift intervals from 0 to 1 identified using the SKA.

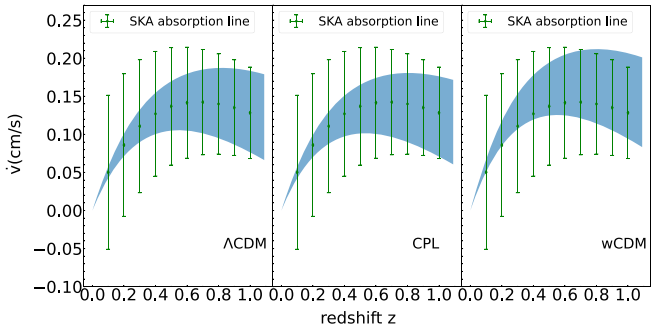

Figure 9. Theoretical velocity variations derived from three distinct models as H_0 varies between 60 and 80 km s^{-1} Mpc^{-1}, depicted within the shallow blue regions. The error bars represent the empirical measurements of redshift drift and velocity drift obtained using the SKA via 21 cm absorption lines over a 0.5 yr observational period within a redshift interval of 0–1.

systems across a redshift interval from 0 to 5 is quantified in a specific functional form, particularly for those exhibiting a H I gas column density of at least 2×10^{20} cm^{-2} (N. Kanekar & F. H. Briggs 2004; S. M. Rao et al. 2017; C.-Z. Lu et al. 2023):

$$n(\mathrm{z}) = dN/dz = (0.027 \pm 0.007)(1+z)^{(1.682\pm0.2)}. \quad (10)$$

The prevalence of DLA systems exhibits an escalation from 97.74 to 276.97 within the redshift interval of 0.1–1, ultimately culminating in a total count of 1818.75. The number density of DLAs is markedly diminished for redshifts less than 1.65. It is well documented that the majority of DLA systems function as substantial repositories of neutral hydrogen in earlier cosmological periods, serving as progenitors to contemporary spiral galaxies. Additionally, the neutral hydrogen mass density contained within DLA systems at a redshift of approximately $z \sim 3$ surpasses the presently observed levels by a factor of roughly 4, paralleling the current stellar mass density observed in star-forming galaxies (N. Kanekar & F. H. Briggs 2004; S. M. Rao et al. 2017).

The quantification of DLA systems enables the determination of the velocity drift ($\dot{v}$) with an associated uncertainty σ_i that scales inversely with the square root of the number of systems, denoted as $1/\sqrt{N}$. Figure 9 presents the projected velocity drift highlighted by green error bars, juxtaposed with the theoretical predictions for the Hubble constant (H_0) shown within the light blue contour map, spanning a magnitude range of 0.05–0.10 cm s^{-1} over an observational period of $\Delta t = 0.5$ yr. The measurement uncertainties, ranging from 0.05 to 0.20 cm s^{-1}, are considerably larger than those obtained from emission data. This disparity is primarily due to the substantially lower number of observed DLA systems compared to the more prevalent H I 21 cm emission line galaxies.

The findings from the constrained analysis are presented in Table 5 and Figures 10 and 11. Compared to the earlier results derived from the emission scenario, where all calculated values of H_0 were below 70 with associated uncertainties not exceeding 1.5, the uncertainties related to the model parameters exhibit a notable increase. The estimations of H_0 now range from 69.57 to 72.59 km s^{-1} Mpc^{-1}, with a minimum uncertainty surpassing 2.8. While Ω_m remains slightly below 0.3, its associated uncertainties have also become more significant. Additionally, the confidence intervals for the dark energy equation-of-state parameters w, w_0, and w_a at 1σ and 2σ deviations have significantly widened compared to the emission scenario results. The observed discrepancy stems from a significant paucity of H I absorption line systems relative to the abundant H I galaxies identified within the sample. Furthermore, to ascertain the constituents and diverse

Table 5
The Best-fit Value and 1σ (68.3%) Uncertainties of H_0 and Ω_m from H I 21 cm Absorption Line Data of SKA in the Three Cosmological Models

Model	H_0	Ω_m	w	w_0	w_a
ΛCDM	$70.71^{+4.881}_{-3.046}$	$0.274^{+0.057}_{-0.048}$	…	…	…
wCDM	$72.59^{+4.102}_{-5.397}$	$0.284^{+0.146}_{-0.261}$	$-0.916^{+0.12}_{-0.107}$	…	…
CPL	$69.57^{+2.822}_{-4.453}$	$0.293^{+0.271}_{-0.195}$	…	$-0.974^{+0.141}_{-0.115}$	$-0.142^{+0.372}_{-0.405}$

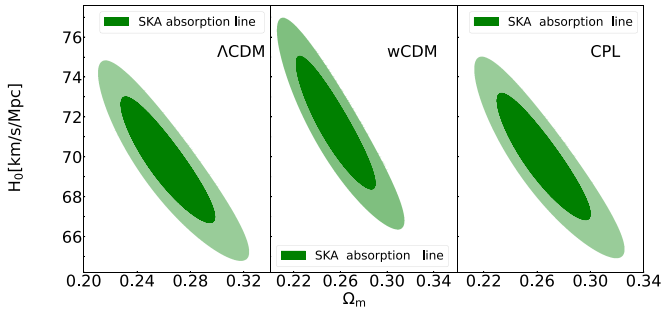

Figure 10. The best-fit value and 1σ (68.3%) and 2σ (95.4%) uncertainties of the H_0–Ω_m plane from SKA absorption line data under the three cosmological models.

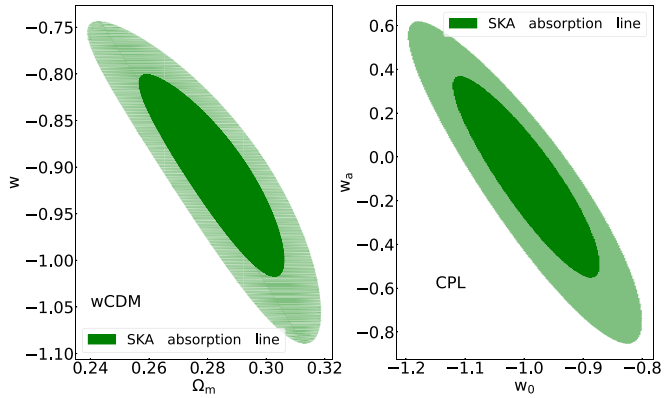

Figure 11. The best-fit value and 1σ (68.3%) and 2σ (95.4%) uncertainties of w and the w_0–w_a plane from SKA absorption line data under the three cosmological models.

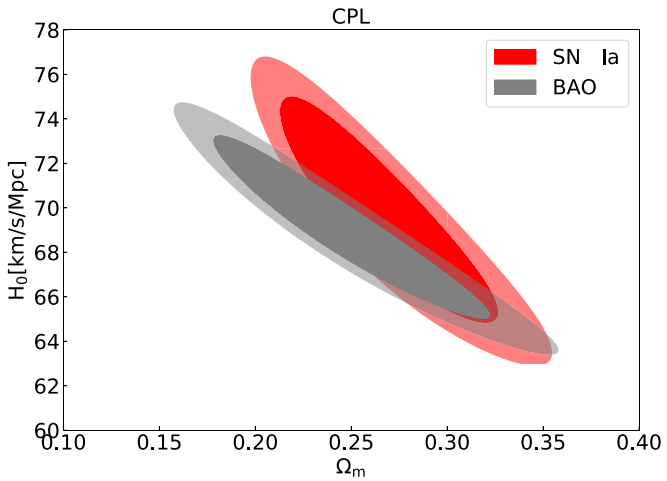

Figure 12. The 1σ (68.3%) and 2σ (95.4%) confidence level of the H_0–Ω_m plane constrained results from SN Ia (red) and BAO (gray) data under the CPL model.

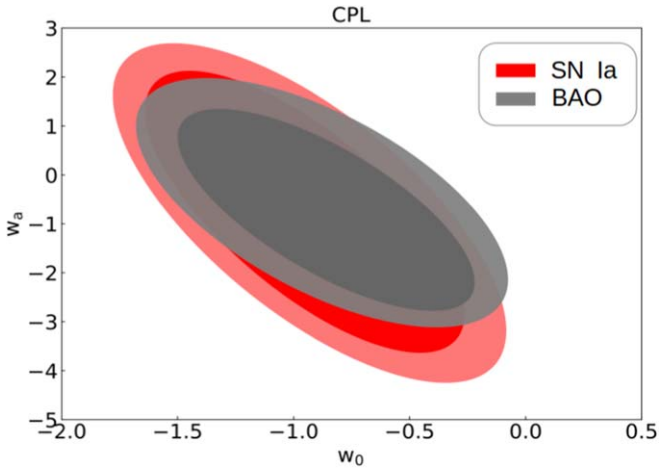

Figure 13. The 1σ (68.3%) and 2σ confidence level of constraints on the w_0–w_a plane using SN Ia (red) and BAO (gray) data under the CPL model.

conditions of the H I gas, it is imperative to analyze the absorption line profiles through the application of multiple Gaussian fitting functions. High-resolution spectral data are essential for an intricate characterization of the H I gas structures detected via SKA's interferometric observations.

To assess the efficacy of redshift drift in constraining cosmological models and parameters, akin to current leading probes such as SN Ia and BAO data sets, Figures 12 and 13 illustrate the constrained cosmological parameters within the CPL framework. According to the SN Ia results (D. M. Scolnic et al. 2018), for the H_0–Ω_m plane, the Hubble constant H_0 resides between 63 and 76.8 km s^{-1} Mpc^{-1} at a 2σ confidence level, while the matter density parameter Ω_m spans from 0.197 to 0.351. In the w_0–w_a parameter space, the constraints are somewhat more relaxed, with w_0 ranging from -1.76 to -0.09 and w_a from -4.84 to 2.79. In comparison to the constrained results derived from 16 BAO data points as referenced in Table 1 of J.-G. Kang et al. (2020), these findings exhibit slightly tighter constraints than those obtained from SNe Ia, despite having fewer data points. Specifically, the Ω_m parameter spans a range from 0.15 to 0.352, which is marginally broader than the SN Ia fits, while the H_0 parameter varies between 64 and 74.6 km s^{-1} Mpc^{-1}. Additionally, w_0 ranges from -1.5 to 0, and w_a ranges from -3.06 to 1.84. Consequently, when integrating the conclusions from the two panels with the aforementioned redshift drift results, the cosmological implications become evident in terms of parameter constraints and precision estimation. This significantly narrows down the parameter ranges and elucidates the nature of dark energy, highlighting the advantages of these observations in cosmological studies.

5. Conclusion

In this investigation, we initially determine the necessary observational accuracy for the cosmological redshift drift, denoted as $\dot{z}$, and the corresponding frequency drift, $\dot{\nu}$, within the context of the ΛCDM paradigm. This precision is assessed over observational time spans of Δt equal to 0.5 and 1 yr, as illustrated in Figure 1, revealing that the redshift variations are approximately 10^{-11} and the frequency shift is below 0.1 Hz for the same astronomical object, resulting in a velocity drift ranging from 0.5 to 3 mm s^{-1} per 0.5 yr. Through a comparative analysis of the measured precision of redshift drift against the H I 21 cm signal detections by the SKA at four distinct high spectral resolutions, namely, 0.001, 0.002, 0.005, and 0.01 Hz, it was ascertained that resolutions at 0.001 Hz and 0.002 Hz suffice to achieve the requisite precision for dimensionless redshift and velocity drift, as demonstrated in Figures 2 and 3 and Table 1. Furthermore, the redshift interval of galaxies detected by the SKA via H I 21 cm line emission in this research can be delineated. Specifically, face-on galaxies exhibiting a distinctive Gaussian flux profile are likely candidates for this signal. The magnitude of velocity drift, along with its associated uncertainties calculated based on the inverse square root of the number of sources ($1/\sqrt{N}$), is illustrated in Figure 4. The observed velocity drift ranges from 0.05 to 0.15 cm s^{-1} per half-year, with corresponding uncertainties of 2–5 mm s^{-1} over a redshift span from 0 to 1. As a result, we utilize these outcomes to enhance the prevailing cosmological models and parameters. The inferred value of H_0 is approximately 70 km s^{-1} Mpc^{-1}, Ω_m remains consistently around 0.3, w is near -1, w_0 is close to -1, and w_a approaches -0.1, regardless of the various models employed. These findings are in strict concordance with previous data. Conversely, the DLA systems, consisting of cold, dense H I gas clouds detectable by the SKA, are not constrained by redshift limitations and exhibit a distinct optical depth signature in the spectra of background quasars or radio galaxies, manifesting as redshifted 21 cm absorption lines. Figure 8 depicts the distribution of DLA systems, along with the precision indicated by the error bars in Figure 9.

The aggregate total of identified DLA systems has reached 1800, which permits the imposition of stringent constraints on cosmological parameters, as illustrated in Figures 10 and 11. In this context, the predicted velocity drift range, characterized by fluctuations from 0.05 to 0.20 cm s^{-1} per 0.5 yr, exhibits marginal uncertainties that are comparatively broader than those inferred from emission data. Nonetheless, the conclusive evidence underscores the singularity of the redshift drift phenomenon as a critical diagnostic tool for advancing cosmological research in the SKA epoch and for deepening our understanding of the fundamental characteristics of dark energy. It is anticipated that the redshift drift signal can be accurately measured at the precision of mm s^{-1} using spectral resolution parameters of 0.001 and 0.002 Hz over an observation duration of $\Delta t = 0.5$ yr. The elucidation of cosmic acceleration driven by dark energy can ultimately be realized through either the analysis of H I 21 cm emissions from galaxies or the examination of the absorption line profiles of DLA systems.

Acknowledgments

This work was supported by the National SKA Program of China (2022SKA0110202) and the China Manned Space Program through its Space Application System.

ORCID iDs

Tong-Jie Zhang https://orcid.org/0000-0002-3363-9965
Ming Zhu https://orcid.org/0000-0001-6083-956X

References

Abdalla, F. B., Bull, P., Camera, S., et al. 2015, in Proc. of Advancing Astrophysics with the Square Kilometre Array (AASKA14) (Giardini Naxos, Italy), 17
Allison, J. R., Sadler, E. M., Amaral, A. D., et al. 2022, PASA, 39, e010
Alves, C. S., Leite, A. C. O., Martins, C. J. A. P., Matos, J. G. B., & Silva, T. A. 2019, MNRAS, 488, 3607
Balbi, A., & Quercellini, C. 2007, MNRAS, 382, 1623
Bolejko, K., Wang, C., & Lewis, G. F. 2019, arXiv:1907.04495
Braun, R., Bonaldi, A., Bourke, T., Keane, E., & Wagg, J. 2019, arXiv:1912.12699
Caldwell, R. R., & Kamionkowski, M. 2009, ARNPS, 59, 397
Cooke, R. 2020, MNRAS, 492, 2044
Cotsakis, S., Mimoso, J. P., & Miritzis, J. 2023, EPJC, 83, 735
Cristiani, S., Boutsia, K., Calderone, G., et al. 2023, arXiv:2302.04365
Darling, J. 2012, ApJ, 761, L26
Dong, C., Gonzalez, A., Eikenberry, S., et al. 2022, MNRAS, 514, 5493
Dutta, R., Kurapati, S., Aditya, J. N. H. S., et al. 2022, JApA, 43, 103
Eden, S. L., Sadler, E. M., Pimbblet, K. A., Mahony, E. K., & Yoon, H. 2025, MNRAS, 536, 387
Esteves, J., Martins, C. J. A. P., Pereira, B. G., & Alves, C. S. 2021, MNRAS, 508, L53
Geréb, K., Maccagni, F. M., Morganti, R., & Oosterloo, T. A. 2015, A&A, 575, A44
Guo, R.-Y., & Zhang, X. 2016, EPJC, 76, 163
Gupta, N., Srianand, R., Noterdaeme, P., Petitjean, P., & Muzahid, S. 2013, A&A, 558, A84
Heinesen, A. 2021, PhRvD, 103, L081302
Jiao, K., Zhang, J.-C., Zhang, T.-J., et al. 2020, JCAP, 2020, 054
Kanekar, N., & Briggs, F. H. 2004, NewAR, 48, 1259
Kanekar, N., & Chengalur, J. N. 2001, A&A, 369, 42
Kanekar, N., Ghosh, T., & Chengalur, J. N. 2001, A&A, 373, 394
Kang, J. 2021, PDU, 31, 100784
Kang, J., Lu, C.-Z., Zhang, T., & Zhu, M. 2023, arXiv:2308.08851
Kang, J., Lu, C.-Z., Zhang, T.-J., & Zhu, M. 2024, RAA, 24, 075002
Kang, J.-G., Gong, Y., Cheng, G., & Chen, X. 2020, RAA, 20, 055
Kim, A. G., Linder, E. V., Edelstein, J., & Erskine, D. 2015, APh, 62, 195
Kloeckner, H. R., Obreschkow, D., Martins, C., et al. 2015, in Proc. of Advancing Astrophysics with the Square Kilometre Array (AASKA14) (Giardini Naxos, Italy), 27
Lane, W., Smette, A., Briggs, F., et al. 1998, AJ, 116, 26
Lazio, J. 2010, PoS, PRA2009, 058
Liske, J., Grazian, A., Vanzella, E., et al. 2008, MNRAS, 386, 1192
Liu, Y., Zhang, J.-F., & Zhang, X. 2020, EPJC, 80, 304
Loeb, A. 1998, ApJL, 499, L111
Lu, C.-Z., Jiao, K., Zhang, T., Zhang, T.-J., & Zhu, M. 2022, PDU, 37, 101088
Lu, C.-Z., Zhang, T., & Zhang, T.-J. 2023, MNRAS, 521, 3150
Martinelli, M., Pandolfi, S., Martins, C. J. A. P., & Vielzeuf, P. E. 2012, PhRvD, 86, 123001
Martins, C. J. A. P., Alves, C. S., Esteves, J., Lapel, A., & Pereira, B. G. 2021, arXiv:2110.12242
Mishra, P., & Célérier Marie-Noëlle Singh, T. P. 2015, Thirteenth Marcel Grossmann Meeting: On Recent Developments in Theoretical and Experimental General Relativity, Astrophysics and Relativistic Field Theories (Singapore: World Scientific Publishing Co.), 1590
Moresco, M., Amati, L., Amendola, L., et al. 2022, LRR, 25, 6
Morganti, R., Sadler, E. M., & Curran, S. 2015, in Proc. of Advancing Astrophysics with the Square Kilometre Array (AASKA14) (Giardini Naxos, Italy), 134
Obreschkow, D., Klöckner, H. R., Heywood, I., Levrier, F., & Rawlings, S. 2009, ApJ, 703, 1890

Perlmutter, S., Turner, M. S., & White, M. 1999, PhRvL, 83, 670
Planck Collaboration, Aghanim, N., Akrami, Y., et al. 2020, A&A, 641, A6
Pritchard, J. R., & Loeb, A. 2012, RPPh, 75, 086901
Quercellini, C., Amendola, L., Balbi, A., Cabella, P., & Quartin, M. 2012, PhR, 521, 95
Rao, S. M., Turnshek, D. A., Sardane, G. M., & Monier, E. M. 2017, MNRAS, 471, 3428
Rawlings, S., & Schilizzi, R. 2011, arXiv:1105.5953
Riess, A. G., Filippenko, A. V., Challis, P., et al. 1998, AJ, 116, 1009
Rocha, B. A. R., & Martins, C. J. A. P. 2023, MNRAS, 518, 2853
Sandage, A. 1962, ApJ, 136, 319
Scolnic, D. M., Jones, D. O., Rest, A., et al. 2018, ApJ, 859, 101
Spekkens, K., Chiang, C., Kothes, R., et al. 2019, Canadian Long Range Plan for Astronomy and Astrophysics White Papers 202046, Zenodo, doi:10.5281/zenodo.3825168
Square Kilometre Array Cosmology Science Working Group, Bacon, D. J., Battye, R. A., et al. 2020, PASA, 37, e007
Staveley-Smith, L., & Oosterloo, T. 2015, in Proc. of Advancing Astrophysics with the Square Kilometre Array (AASKA14) (Giardini Naxos, Italy), 167
Wolfe, A. M. 1988, in Proc. of the QSO Absorption Line Meeting, ed. J. C. Blades, D. A. Turnshek, & C. A. Norman (Cambridge: Cambridge Univ. Press), 297
Yahya, S., Bull, P., Santos, M. G., et al. 2015, MNRAS, 450, 2251
Yoon, H., Sadler, E. M., Mahony, E. K., et al. 2024, arXiv:2408.06626
Yu, H.-R., Zhang, T.-J., & Pen, U.-L. 2014, PhRvL, 113, 041303